

Microscopy on Thermal Capillary Waves in Demixed Colloid-Polymer Systems

Dirk G. A. L. Aarts¹, Matthias Schmidt²,
Henk N. W. Lekkerkerker¹, and Klaus R. Mecke³

¹ Van't Hoff Laboratory, Debye Institute, Utrecht University,
Padualaan 8, 3584 Utrecht, The Netherlands

² Institut für Theoretische Physik II, Heinrich-Heine-Universität Düsseldorf,
Universitätsstraße 1, 40225 Düsseldorf, Germany

³ Institut für Theoretische Physik, Universität Erlangen,
Staudtstrasse 7, 91058 Erlangen, Germany

Summary. Recently we have shown how to tune length- and timescales in demixed colloid-polymer dispersions in such a way that thermal capillary waves at the free interface between demixed fluid phases can be studied directly by means of laser scanning confocal microscopy [Aarts, Schmidt and Lekkerkerker, *Science* **304**, 847 (2004)]. Here, we focus on several static properties of the interface. We show that the probability of fluctuations of the local interface position around its equilibrium value is Gaussian. By comparing two-point correlations of these fluctuations as a function of distance with predictions from capillary wave theory, we obtain results for the interfacial tension and the capillary length. The presented technique enables us to measure also the probability distribution of the tilt angle of the local interface normal and the vertical direction.

1 Introduction

A few years after Einstein's famous 1905 theory of Brownian motion [1] Smoluchowski used molecular kinetic theory to give the first correct explanation of critical opalescence [2]. In the same paper Smoluchowski indicated that due to the thermal motion of the molecules the free interface between two fluids, like that between a liquid and a vapor, inevitably becomes rough. Using the thermodynamic fluctuation theory developed by Einstein in 1910 [3] Mandelstam developed the ideas of Smoluchowski in a quantitative theory in terms of thermal capillary waves [4]. The Smoluchowski-Mandelstam theory was rediscovered by Buff, Lovett and Stillinger [5]. As remarked by Mandelstam it is rare that the circumstances are so favorable that the expected thermal fluctuations indeed can be observed. One such case, in which nowadays direct observations are relatively straightforward, is the Brownian motion. In the period 1908-1915 Perrin was able to make observations in simple, brilliant experiments that confirmed the theory of Einstein and led to the determination of Avogadro's number [6]. The direct observation of critical fluctuations had to wait till 1966 and was the last preoccupation by Debye [7]. Beysens and co-workers did further work on this topic [8]. Clearly, direct observations

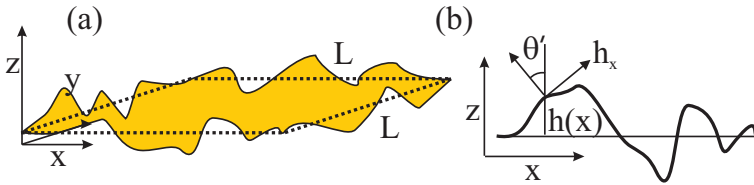


Fig. 1. (a) Schematic depiction of a curved interface. A point at the interface \mathbf{r} is written in terms of $(x, y, h(x, y))$. (b) A 2D slice out of (a). The projected angle θ' is related to the interface derivative h_x via $h_x = \tan \theta'$

may help to answer basic questions and the direct visual observation of thermal capillary waves that will be reported in this contribution proved to be very rich indeed [9]. Here, we show that in demixed colloid-polymer dispersions the thermal fluctuations of the fluid-fluid interface can be seen directly in real space and we will discuss the static properties of these fluctuations.

The article is organized as follows; We start with a brief derivation of capillary wave theory in Section 2 deriving the relevant expressions that we use to analyze our data, followed by a description of the experimental system and the experimental methods in Section 3. Results are given in Section 4 and conclusions and an outlook are presented in Section 5.

2 Theoretical Background

We here follow the statistical analysis of interface corrugations, first developed by Mandelstam [4], as reviewed by Vrij [10]. The work ΔF to create a corrugation at constant temperature can be written as

$$\Delta F = \Delta F_g + \Delta F_c, \quad (1)$$

where we only consider gravity (ΔF_g) and capillary (ΔF_c) forces, resulting from the displacement of matter against gravity and the creation of extra interface area, respectively. Other contributions, for example arising from bending of the interface, are ignored, the validity of which will be discussed in Section 5. Clearly, this is a mesoscopic approach, which is justified if one looks at distortions much larger than the particle size as is done in light scattering studies on molecular interfaces. The local interface position with respect to the mean interface position has coordinates $\mathbf{r} = (x, y, h(x, y))$, see Fig. 1. This Monge parameterization neglects overhang of the interface as well as bubbles of one phase in the other. To create a corrugation of an area $dx dy$ over a distance h gravity contributes

$$\delta F_g = \int_0^h h' g \Delta \rho dx dy dh' = \frac{1}{2} g \Delta \rho h^2 dx dy \quad (2)$$

with g Earth's acceleration, and $\Delta \rho$ the mass density difference. The interfacial tension γ contributes

$$\delta F_c = \gamma \Delta A = \gamma dx dy \left(\sqrt{1 + h_x^2 + h_y^2} - 1 \right) \approx \frac{1}{2} \gamma dx dy (h_x^2 + h_y^2), \quad (3)$$

with $h_i \equiv \partial h / \partial i$ and $i = x, y$. Integrating over the total interface area $L \times L$ gives

$$\Delta F_g = \frac{1}{2} g \Delta \rho \int \int dx dy h^2, \quad (4)$$

and

$$\Delta F_c = \frac{1}{2} \gamma \int \int dx dy (h_x^2 + h_y^2). \quad (5)$$

The height h can be expanded in a Fourier series in a square with length L ,

$$h = \sum_{\mathbf{k}} h_{\mathbf{k}} e^{i(k_x x + k_y y)}, \quad (6)$$

with $h_{\mathbf{k}}$ the Fourier coefficients and $\mathbf{k} = (k_x, k_y)$. The summation runs over all Fourier modes k_x and k_y . From Parseval's identity one readily obtains

$$\Delta F = \frac{1}{2} L^2 \sum_{\mathbf{k}} |h_{\mathbf{k}}|^2 (g \Delta \rho + \gamma k^2), \quad (7)$$

with $k^2 = k_x^2 + k_y^2$ and $k = |\mathbf{k}|$. Mandelstam made use of the equipartition theorem which states that the work necessary to create each mode is equal to $k_B T / 2$, with k_B Boltzmann constant and T the absolute temperature. Thus, in the capillary wave spectrum each Fourier component $h_{\mathbf{k}}$ of the interface displacement contributes

$$\langle |h_{\mathbf{k}}|^2 \rangle = \frac{k_B T}{\gamma L^2} \frac{1}{k^2 + L_{\parallel}^{-2}}, \quad (8)$$

where the brackets on the left hand side denote a thermal average and L_{\parallel} is the lateral correlation length. It is given through

$$L_{\parallel} = \sqrt{\gamma / (g \Delta \rho)}. \quad (9)$$

When an external wall is additionally taken into account, L_{\parallel} is the characteristic (capillary) length of the meniscus [11, 12, 13]. From (8) and again applying Parseval's theorem the mean square interfacial roughness is found to be

$$\langle h^2 \rangle = \frac{k_B T}{4\pi\gamma} \ln \left[\frac{k_{max}^2 + L_{\parallel}^{-2}}{k_{min}^2 + L_{\parallel}^{-2}} \right], \quad (10)$$

with $k_{min} = 2\pi/L$ and $k_{max} = 2\pi/l_m$. L denotes the physical system size and l_m is a microscopic length [5]. Thus, the interfacial roughness $L_{\perp} \equiv \sqrt{\langle h^2 \rangle}$ is proportional to $\sqrt{k_B T / \gamma}$.

Since the interface is constantly subject to random forces the distribution $P(h)$ of the interface heights is described by a Gaussian with (10) its variance σ^2 . This means the distribution is given by

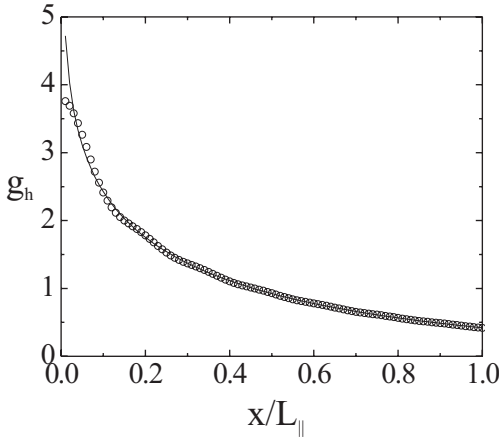


Fig. 2. Static height correlation functions g_h as a function of x/L_{\parallel} in units of $k_B T/2\pi\gamma$. The symbols denote calculations in which $\bar{k}_{max} = 44$, the full curve is for $\bar{k}_{max} = \infty$

$$P(h) = \frac{1}{\sqrt{2\pi\sigma^2}} e^{-h^2/2\sigma^2}. \quad (11)$$

Further information on the physical properties of the interface can be obtained by considering correlation functions. The static height-height correlation function at a given time t is constructed as

$$g_h(x) = \langle h(x', t') h(x' + x, t') \rangle. \quad (12)$$

The angular brackets denote averages over primed quantities. Although we have experimental data only for the x - and not for the y -dependence, as will be shown below, this contains the full information due to the cylindrical symmetry of the interface around the vertical z -direction. It is therefore possible to obtain all information just by performing the analysis along one dimension. The correlation function is obtained by Fourier transforming (8). We can write

$$g_h(x) = \sum_{\mathbf{k}} \frac{k_B T}{\gamma L^2} \frac{1}{k^2 + L_{\parallel}^{-2}} e^{i\mathbf{k}\cdot\mathbf{s}} = \frac{k_B T}{\gamma L^2} \frac{L^2}{(2\pi)^2} \int d\mathbf{k} \frac{1}{k^2 + L_{\parallel}^{-2}} e^{i\mathbf{k}\cdot\mathbf{s}}, \quad (13)$$

where we have switched from a summation to an integration and $\mathbf{s} = (x, y)$. Next, we change to cylindrical coordinates and perform the integration over ϕ and obtain

$$\begin{aligned} g_h &= \frac{k_B T}{\gamma} \frac{1}{(2\pi)^2} \int dk \frac{k}{k^2 + L_{\parallel}^{-2}} \int_0^{2\pi} d\phi e^{ikx \cos \phi} \\ &= \frac{k_B T}{\gamma} \frac{2\pi}{(2\pi)^2} \int dk \frac{k}{k^2 + L_{\parallel}^{-2}} J_0(kx). \end{aligned} \quad (14)$$

The symbol J_0 denotes the Bessel function of the first kind. The integration over k is performed from k_{min} to k_{max} , see just below (10). We can directly set k_{min} to zero, since $2\pi/L \sim 0$. Setting k_{max} to ∞ allows performing the integration and (14) then becomes

$$g_h(x) = \frac{k_B T}{2\pi\gamma} K_0 \left(\frac{x}{L_{\parallel}} \right), \quad (15)$$

where K_0 is the modified Bessel function of the second kind as a function of x/L_{\parallel} . We can test the effect of setting k_{max} to infinity. We change to $\bar{k} = kL_{\parallel}$ in (14) and use $k_{max} = 2\pi/\sigma_c$ as a reasonable cutoff with σ_c the colloid diameter. As will be shown below L_{\parallel} is at least a couple of microns and here we will fix it at a minimal value of 1 μm , whereas $\sigma_c = 142$ nm, such that \bar{k}_{max} is at least ~ 44 . In Fig. 2(a) we plot results from equation (14) with $\bar{k}_{max} = 44$ and equation (15). Only at a distance $x/L_{\parallel} < 0.05$ clear differences can be observed between the two functions. Furthermore, the curve obtained with finite cut-off shows some fine structure. We thus conclude that (15) holds for distances x larger than a small-distance cutoff of the order of the particle size.

A natural extension of the above framework is to analyze the distribution of the angle between the local interface normal and the vertical direction [14], i.e. the tilt angle distribution. This is related to derivatives of h in the x -direction: h_x . Again, the distribution of h_x is Gaussian. The derivative stands in direct connection to the (projected) angle θ' normal to the interface, $h_x = \tan \theta$ (see Fig. 1(b)). It can be shown that the distribution in one dimension is given by [14]

$$P(\theta') = \frac{2}{\sqrt{2\pi\sigma'^2}} \frac{e^{-\frac{1}{2} \frac{\tan^2 \theta'}{\sigma'^2}}}{\cos^2 \theta'} \quad (16)$$

with $\sigma'^2 \equiv \langle \tan^2 \theta \rangle$ the variance. The special form of this equation is a result of the Jacobian of the transformation of h_x to θ using $\partial h_x(\theta)/\partial \theta = 1/\cos^2 \theta$. The variance is extremely sensitive to the value of k_{max} [14].

In molecular fluids γ is of the order of 10 – 100 mN/m and $\Delta\rho$ is about $10^2 - 10^3$ kg/m³. Therefore, the interface roughness $L_{\perp} \sim 0.3$ nm, whereas the correlation length $L_{\parallel} \sim 3$ mm resulting in extreme ratios of roughness-to-correlation length of 10^{-7} , only accessible through scattering techniques. Here we exploit the scaling up of lengths when going from molecules to mesoscopic colloidal particles of size 140 nm in order to directly observe capillary waves in real space.

Adding polymer to a colloidal suspension may induce a fluid-fluid demixing transition that is widely accepted to be the mesoscopic analogue of the liquid-gas phase transition in atomic substances [15, 16]. The coexisting phases are a colloidal liquid (rich in colloid and poor in polymer) and a colloidal gas (poor in colloid and rich in polymer). The origin of the phase separation lies in the entropy-driven attraction between the colloids, which is mediated by the polymers [17, 18]. It is known from experiment [19, 20, 21, 11, 9],

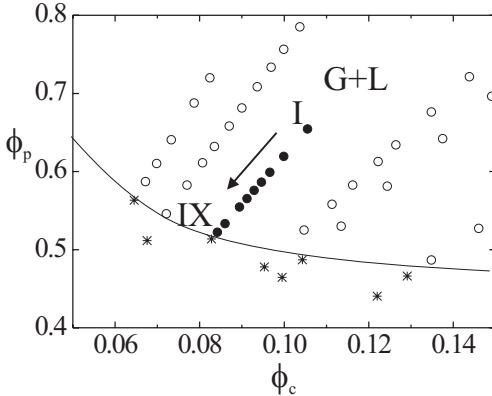


Fig. 3. Phase diagram in (ϕ_p, ϕ_c) -representation. Indicated are state points where gas-liquid phase separation occurs (open and filled circles) and state points in the one-phase region (crosses). The line is an estimate of the binodal and is drawn to guide the eye. State points I-IX (filled circles) are indicated

theory [22, 23, 24, 25, 26] and simulations [27, 28], that in such systems the interfacial tension scales as $\gamma \sim k_B T / \sigma_c^2$ leading to ultra-low values for γ ($\sim 1 \mu\text{N/m}$ and below). This, in turn, implies that using colloidal suspensions scales up the interface roughness and simultaneously scales down the correlation length. With the current system (as detailed below) we succeed to bring both the roughness and the correlation length in the μm -regime. In addition, the interplay between ultra-low interfacial tension and relatively large viscosity, η , sets the capillary velocity γ/η (see for example [29]) in the range of $\mu\text{m/s}$, as opposed to typical velocities of the order of 10 m/s in molecular fluids. The associated characteristic time for the decay of interfacial fluctuations, which we refer to as the capillary time, is given by $\tau = L_{\parallel} \eta / \gamma$. In the case of colloids it becomes of the order of seconds. Thus, through the appropriate choice of the colloid diameter we can trace the statics *and* dynamics of the capillary waves at a free interface with optical microscopy [9], but here we will restrict ourselves to the statics.

3 Experimental Methods

We used fluorescently labeled poly(methylmethacrylate) (PMMA) colloidal spheres [30] with radius of $R_c = 71 \text{ nm}$ (obtained from static light scattering) and size polydispersity of less than 10%. The polymer was commercially available polystyrene (Fluka) with molecular weight $M_w = 2 \cdot 10^6 \text{ g mol}^{-1}$ ($M_w/M_n < 1.2$, where M_n is the number average molecular weight) and radius of gyration of $R_g \sim 44 \text{ nm}$ (estimated from data in the literature [31, 32]).

Thus the size ratio, $R_g/R_c = 0.6$, was sufficiently large to obtain stable fluid-fluid demixing [33]. Both species were dispersed in cis/trans-decalin and since all densities were known, mass fractions could be directly converted to packing fractions of colloids, $\phi_c = \frac{4}{3}\pi R_c^3 n_c$, and polymers, $\phi_p = \frac{4}{3}\pi R_g^3 n_p$, where n_c and n_p are the number densities of colloids and polymers, respectively. Samples were prepared by mixing colloid and polymer stock dispersions and diluting with decalin in order to control the overall packing fractions ϕ_c and ϕ_p . The underlying phase diagram is shown in Fig. 3. Large glass cuvettes (of volume $\sim 1 \text{ cm}^3$) with extra thin (thickness of 0.17 mm) cover glass walls were used. A confocal scanning laser head (Nikon C1) was mounted on a horizontally placed light microscope (Nikon Eclipse E400). Each measurement was done after one day of equilibration. The microscope was aligned by making use of the interface which serves as a spirit level. We checked that the system was well equilibrated by following the recovery of intensity after bleaching a space region in the gas and/or liquid phase. The recovery appeared to be governed solely through diffusion of particles without any indications of drift (e.g. through convection). Different data sets were acquired at many different state points following several dilution lines. The data sets consisted of approximately $5.1 \cdot 10^5$ interface data points when images were scanned as fast as possible (about 5 frames per second), and about $1.5 \cdot 10^5$ when a delay time between consecutive images was used (of about 10 s) to get rid of some of the time correlation.

Pictures, such as those in Fig. 4, represent an intensity distribution of fluorescent light, $I(x, z, t)$, at a certain time t with x the horizontal (along the interface) and z the vertical (opposite to gravity) components of the space vector. The microscope records the fluorescence of excited dye within the colloids, hence the colloid-rich (liquid) phase appears bright and the colloid-poor (gas) phase appears dark. $I(x, z, t)$ is a direct measure of the local and instantaneous distribution of colloidal particles and provides the starting point for a statistical analysis. Due to the finite resolution [34, 35] we can access length scales $\sim 2R_c$, and we neglect effects induced by the finite time needed to scan each frame, and take I as an instantaneous snapshot (justified by comparing the colloid self-diffusion time with the scanning time). Thus, the real space pictures in Fig. 4 show the structure of a gas-liquid interface practically at the particle scale. We rely on the concept of a local interface between both phases. In the spirit of a Gibbs dividing surface we define an interface position $h_b(x, t)$ (now with respect to the bottom of the image, instead of the mean interface position as in Section 2) such that in one column of vertical length L_z the total intensity can be written as

$$\int_0^{L_z} dz I(x, z, t) = I_{\text{liq}}(x) h_b(x, t) + I_{\text{gas}}(x) (L_z - h_b(x, t)) \quad (17)$$

Here, the values $I_{\text{gas}}(x)$ and $I_{\text{liq}}(x)$ are the average bulk intensities in the gas and liquid phase, respectively, and are taken to be functions of x to account for the microscope objective properties. In practice, integrals in the notation

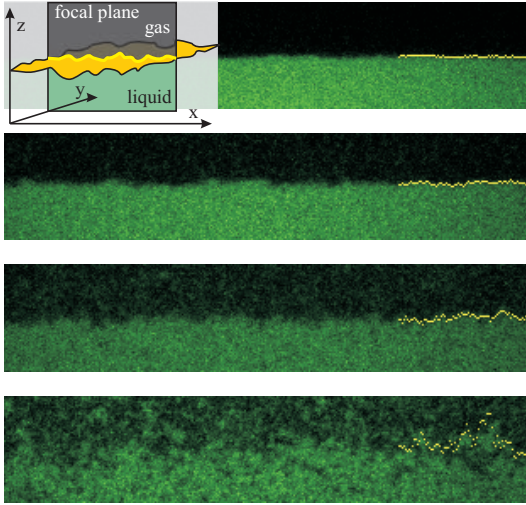


Fig. 4. Capillary waves at the free liquid-gas interface in a phase-separated colloid-polymer mixture imaged with laser scanning confocal microscopy (LSCM) at four different state points approaching the critical point (from top to bottom: state points I, VI, VIII and IX, see Fig. 3). The focal (viewing) plane is perpendicular to the interface and only a very thin slice (of thickness $\sim 0.6 \mu\text{m}$) is imaged (see the inset). Gravity points downwards and the size of each image is $17.5 \times 85 \mu\text{m}^2$. Thermally excited capillary waves corrugate the interface and their amplitude increases upon approaching the critical point. The bright dots at the right indicate the surface location $h(x)$ obtained with our method

are sums over pixels and we have checked that the results of the subsequent analysis in correlation functions do not depend sensitively on the precise definitions of I_{gas} and I_{liq} . The resulting “height” function $h_b(x)$ (shown as the bright spots in Fig. 4) describes the interface position quite accurately. From top to bottom in Fig. 4 we approach the critical point and both the capillary waves and density fluctuations increase, while the density (intensity) difference between the two phases decreases. For each frame the average interface position is $\bar{h}_b(t) \equiv \langle h_b(x', t) \rangle$, in which the angular brackets denote averages over primed quantities. We now define a new height function that describes the deviations from the mean interface position $h(x, t) = h_b(x, t) - \bar{h}_b(t)$.

4 Results and Discussion

The distribution of heights is shown in Fig. 5 for three different state points. The width of the distribution for state point I is about twice the particle diameter, the order of which is in good agreement with (10). As one approaches the critical point the distributions get broader up to 7 times the

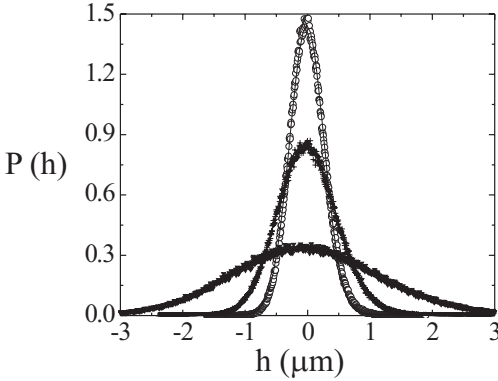


Fig. 5. Distribution of height values, $P(h)$, for three different state points: I (open circles), V (plusses) and VIII (triangles). Full curves are Gaussian fits (11)

particle diameter for state point VIII, but the shape remains that of a normal distribution. However, the physical interpretation of this figure is limited due to the finite resolution of the confocal technique as well as our interface location procedure. Each height $h(x, t)$ appears to consist of the actual height plus a delta correlated “noise” term $\Delta(x, t)$ with properties such that $\langle \Delta(x', t') \rangle = 0$, and $\langle h(x', t') \Delta(x', t') \rangle = 0$ averaged over either x' or t' . Furthermore, $\langle \Delta(x', t') \Delta(x' + x, t' + t) \rangle = \sigma_{\Delta}^2 \delta(x) \delta(t)$ with δ the delta function. Thus, from Fig. 5 we see that the interface roughness is Gaussian, but the actual physics – although present as can be observed from the trends in the figure – is blurred by the small noise term. To cope with the delta-correlated noise we construct a correlation function, which clearly does not suffer from such noise, except when both $x = 0$ and $t = 0$.

The static correlation function (equation (15)) describes the experimental data points very well, as can be seen in Fig. 6 for various state points with only two physical parameters γ and L_{\parallel} . No bending term in (8) was needed in the analysis. Note that in the original paper [9] the y-axis was given in units of pixel area and not (as indicated) in μm^2 , but the analysis was not affected by this. Results for the interfacial tension and the capillary length are displayed in Fig. 7(a) and (b).

To further explore the properties of the interface we examine derivatives of $h(x, t)$ [14]. In Fig. 8 histograms are plotted of the absolute value of θ' for three different state points (as in Fig. 5). One can either use (16) to fit to the data with the variance as fitting parameter or obtain the variance directly from the experiment. In Fig. 8 both methods are plotted. The agreement is yet another confirmation that the interface can be described within a Gaussian interface model. As the critical point is approached the peak in the angle distribution shifts from 0° to 75° , since the interface roughness

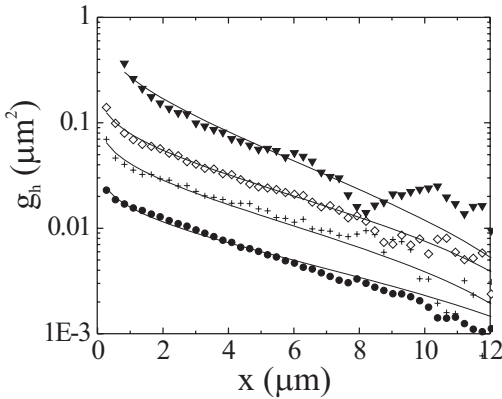


Fig. 6. Static height-height correlation function $g_h(x)$ as obtained from quantitative analysis of LSCM pictures as a function of the (lateral) distance x for state points I, V, VI and VIII (see Fig. 3) approaching the critical point from bottom to top. Experimental results (symbols) are compared with predictions from the capillary wave model (lines)

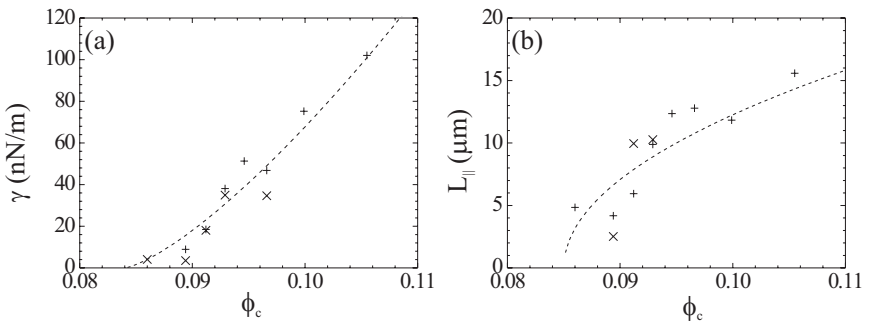


Fig. 7. (a) Interfacial tension γ as a function of the overall colloid packing fraction ϕ_c obtained from $g_h(x)$ (crosses: slow frame rate, pluses: fast frame rate). (b) The capillary length L_{\parallel} as a function of ϕ_c obtained from $g_h(x)$. Results stem from state points on the same dilution line as state points I-IX. The dashed lines are to guide the eye

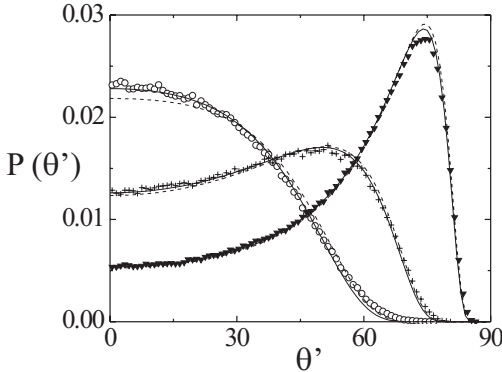


Fig. 8. Angle distributions for three different state points: I (open circles), V (plusses) and VIII (triangles). We either fitted the variance in (16) (full curves) or obtained the variance directly from experiment (dashed curves)

increases and the correlation length decreases. As σ'^2 depends strongly on the molecular interactions, it is in principle possible to obtain the interfacial tension more accurately and to determine the microscopic cut-off k_{max} , i.e. the microscopic length l_m in (10) [14]. It could be interesting if on the particle level a wave-vector dependent surface tension can be detected due to molecular interactions, as predicted for simple liquids [36], and observed in various liquids [37, 38].

5 Conclusions

Using a colloid-polymer mixture allows to carefully tune the interface properties and as a result the thermal capillary waves at a free interface are observed visually by means of LSCM. From the fluorescence intensity difference between the two phases the interface can easily be located and the height functions are constructed. By analyzing the height fluctuations of the interface position as well as the derivatives of these we see that the interface roughness can be described within a Gaussian model. To deal with small noisy contributions to the height function correlation functions are determined. The quality of the fits to describe the correlation functions validate the capillary wave model practically down to the particle level.

The present work opens up a wide range of possibilities, e.g. to study the interface at a particle level by using even larger colloids, explore temperature gradients and mass transport across the interface, and the effects on droplet coalescence [9] and snap-off, on heterogeneous catalysis, freezing of capillary waves at the gel-line, the effects of thermal capillary waves on wetting properties etc.

Acknowledgements

This work was supported by the Stichting voor Fundamenteel Onderzoek der Materie (Foundation for Fundamental Research on Matter), which is part of the Nederlandse Organisatie voor Wetenschappelijk Onderzoek (Netherlands Organisation for Advancement of Research), and we also acknowledge financial support by the DFG SFB TR6 “Colloidal dispersions in external fields”.

References

1. A. Einstein, *Ann. Phys.* **17**, 549 (1905). 15
2. M. V. von Smoluchowski, *Ann. Phys.* **25**, 205 (1908). 15
3. A. Einstein, *Ann. Phys.* **33**, 1275 (1910). 15
4. L. Mandelstam, *Ann. Phys.* **41**, 609 (1913). 15, 16
5. F. P. Buff, R. A. Lovett, and F. H. Stillinger, *Phys. Rev. Lett.* **15**, 621 (1965). 15, 17
6. J. Perrin, *Ann. de Chim. Phys.* **18**, 5 (1909). 15
7. P. Debye and R.T. Jacobson, *J. Chem. Phys.* **48**, 203 (1968). 15
8. P. Guenon, F. Perrot, and D. Beysens, *Phys. Rev. Lett.* **63**, 1152 (1989). 15
9. D. G. A. L. Aarts, M. Schmidt, and H. N. W. Lekkerkerker, *Science* **304**, 847 (2004). 16, 19, 20, 23, 25
10. A. Vrij, *Adv. Coll. Interf. Sci.* **2**, 39 (1968). 16
11. D. G. A. L. Aarts, J. H. van der Wiel, and H. N. W. Lekkerkerker, *J. Phys.: Condens. Matter* **15**, S245 (2003). 17, 19
12. D. G. A. L. Aarts and H. N. W. Lekkerkerker, *J. Phys.: Condens. Matter* **16**, S4231 (2004). 17
13. D. G. A. L. Aarts, *J. Phys. Chem. B* **109**, 7407 (2005). 17
14. K.R. Mecke and S. Dietrich, preprint, cond-mat/0505294 (2005). 19, 23, 25
15. W.C.K. Poon, *J. Phys.: Condens. Matter* **14**, R859 (2002). 19
16. R. Tuinier, J. Rieger, and C.G. de Kruif, *Adv. Coll. Interf. Sci.* **103**, 1 (2003). 19
17. S. Asakura and F. Oosawa, *J. Chem. Phys.* **22**, 1255 (1954). 19
18. A. Vrij, *Pure Appl. Chem.* **48**, 471 (1976). 19
19. E. H. A. de Hoog and H. N. W. Lekkerkerker, *J. Phys. Chem. B* **103**, 5274 (1999). 19
20. B. H. Chen, B. Payandeh, and M. Robert, *Phys. Rev. E* **62**, 2369 (2000). 19
21. E. H. A. de Hoog and H. N. W. Lekkerkerker, *J. Phys. Chem. B* **105**, 11636 (2001). 19
22. A. Vrij, *Physica A* **235**, 120 (1997). 20
23. J. M. Brader and R. Evans, *Europhys. Lett.* **49**, 678 (2000). 20
24. J. M. Brader, R. Evans, M. Schmidt, and H. Löwen, *J. Phys.: Condens. Matter* **14**, L1 (2002). 20
25. A. Moncho-Jorda, B. Rotenberg, and A. A. Louis, *J. Chem. Phys.* **119**, 12667 (2003). 20
26. D. G. A. L. Aarts, R. P. A. Dullens, H. N. W. Lekkerkerker, D. Bonn, and R. van Roij, *J. Chem. Phys.* **120**, 1973 (2004). 20

27. R. L. C. Vink and J. Horbach, *J. Chem. Phys.* **121**, 3253 (2004). 20
28. R. L. C. Vink and J. Horbach, *J. Phys.: Condens. Matter* **16**, S3807 (2004). 20
29. R. F. Probstein, *Physicochemical Hydrodynamics*, section 10.2, (John Wiley & Sons, Hoboken 2003). 20
30. G. Bosma, C. Pathmamanoharan, E. H. A. de Hoog, W. K. Kegel, A. van Blaaderen, and H. N. W. Lekkerkerker, *J. Colloid Interface Sci.* **245**, 292 (2002). 20
31. G.C. Berry, *J. Chem. Phys.* **44**, 4550 (1966). 20
32. B. Vincent, *Colloids Surf.* **50**, 241 (1990). 20
33. H. N. W. Lekkerkerker, W. C. K. Poon, P. N. Pusey, A. Stroobants, and P. B. Warren, *Europhys. Lett.* **20**, 559 (1992). 21
34. T. Wilson, *Confocal Microscopy*, (Academic Press Ltd., London 1990). 21
35. R. H. Webb, *Rep. Prog. Phys.* **59**, 427 (1996). 21
36. K. R. Mecke and S. Dietrich, *Phys. Rev. E* **59**, 6766 (1999). 25
37. C. Fradin, A. Braslau, D. Luzet, D. Smilgies, M. Alba, N. Boudet, K. R. Mecke, and J. Daillant, *Nature* **403**, 871 (2000). 25
38. S. Mora, J. Daillant, K. R. Mecke, D. Luzet, A. Braslau, M. Alba, and B. Struth, *Phys. Rev. Lett.* **90**, 216101 (2003). 25